



THE UNIVERSITY *of* EDINBURGH

Edinburgh Research Explorer

A Physical Impact of Organic Fouling Layers on Bacterial Adhesion During Nanofiltration

Citation for published version:

Heffernan, R, Habimana, O, Semiao, A, Cao, H, Safari, A & Casey, E 2014, 'A Physical Impact of Organic Fouling Layers on Bacterial Adhesion During Nanofiltration', *Water Research*, vol. 67, pp. 118–128.
<https://doi.org/10.1016/j.watres.2014.09.012>

Digital Object Identifier (DOI):

[10.1016/j.watres.2014.09.012](https://doi.org/10.1016/j.watres.2014.09.012)

Link:

[Link to publication record in Edinburgh Research Explorer](#)

Document Version:

Early version, also known as pre-print

Published In:

Water Research

General rights

Copyright for the publications made accessible via the Edinburgh Research Explorer is retained by the author(s) and / or other copyright owners and it is a condition of accessing these publications that users recognise and abide by the legal requirements associated with these rights.

Take down policy

The University of Edinburgh has made every reasonable effort to ensure that Edinburgh Research Explorer content complies with UK legislation. If you believe that the public display of this file breaches copyright please contact openaccess@ed.ac.uk providing details, and we will remove access to the work immediately and investigate your claim.



A Physical Impact of Organic Fouling Layers on Bacterial Adhesion During Nanofiltration

R. Heffernan¹, O. Habimana¹, A.J.C. Semião², H. Cao¹, A. Safari¹ and E. Casey^{1*}

¹*School of Chemical and Bioprocess Engineering, University College Dublin, Co. Dublin, Ireland*

²*School of Engineering, The University of Edinburgh, Edinburgh, United Kingdom*

*eoin.casey@ucd.ie

*Corresponding author. Mailing address: University College Dublin, School of Chemical and
Bioprocess Engineering, Belfield, Dublin 4, IRELAND. Phone: +353 1 716 1877, Email:
eoin.casey@ucd.ie

Abstract

Organic conditioning films have been shown to alter properties of surfaces, such as hydrophobicity and surface free energy. Furthermore, initial bacterial adhesion has been shown to depend on the conditioning film surface properties as opposed to the properties of the virgin surface. For the particular case of nanofiltration membranes under permeate flux conditions, however, the conditioning film thickens to form a thin fouling layer. This study hence sought to determine if a thin fouling layer deposited on a nanofiltration membrane under permeate flux conditions governed bacterial adhesion in the same manner as a conditioning film on a surface.

Thin fouling layers (less than 50 μm thick) of humic acid or alginic acid were formed on Dow Filmtec NF90 membranes and analysed using Atomic Force Microscopy (AFM), Confocal Microscopy and surface energy techniques. Fluorescent microscopy was then used to quantify adhesion of *Pseudomonas fluorescens* bacterial cells onto virgin or fouled membranes under filtration conditions.

It was found that instead of adhering on or into the organic fouling layer, the bacterial cells penetrated the thin fouling layer and adhered directly to the membrane surface underneath. Contrary to what surface energy measurements of the fouling layer would indicate, bacteria adhered to a greater extent onto clean membranes (24 ± 3 % surface coverage) than onto those fouled with humic acid (9.8 ± 4 %) or alginic acid (7.5 ± 4 %). These results were confirmed by AFM measurements which indicated that a considerable amount of energy (10^{-7} J/ μm) was dissipated when attempting to penetrate the fouling layers compared to adhering onto clean NF90 membranes (10^{-15} J/ μm). The added resistance of this fouling layer was thusly seen to reduce the number of bacterial cells which could reach the membrane surface under permeate conditions.

46 This research has highlighted an important difference between fouling layers for the
47 particular case of nanofiltration membranes under permeate flux conditions and surface
48 conditioning films which should be considered when conducting adhesion experiments under
49 filtration conditions. It has also shown AFM to be an integral tool for such experiments.

50 *Key words: Fouling layer, natural organic matter, atomic force microscopy, nanofiltration,*
51 *bacterial adhesion*

1. Introduction

Since the first large-scale application at the Méry-sur-Oise water filtration plant in France (Cyna et al. 2002), nanofiltration (NF) has become a proven method of water purification. It provides an efficient method of cleaning water of metals, organic matter, organic trace contaminants and divalent salts. However, as these are retained by the NF membrane they build up on the membrane's surface forming a fouling layer which reduces membrane performance (Yuan and Kilduff 2010). Fouling remains the biggest obstacle for the NF industry today.

Bacteria present in the water and retained by the NF membrane threaten the most damaging form of fouling: biofouling. As bacteria adhere to the membrane's surface they bind together, excreting exopolymetric substances (EPS) forming a communal film: biofilm (Flemming 1997). Bacteria within the biofilm grow and proliferate, expanding the biofilm's influence and further reducing the membrane's filtration capacity (Vrouwenvelder et al. 2008). Bacteria dissociating from mature biofilms pose a threat to further membrane modules or other processes downstream.

Efforts to combat this biofouling phenomenon have focused on three approaches: removal, nutrient removal and prevention. The first seeks a method by which existing biofilms can be detached or eliminated, restoring the performance of biofouled membranes using surfactants, chelating agents, chaotropic agents, chlorinated compounds or enzymes (Chen and Stewart 2000, Liikanen et al. 2002). The second limits the amount of nutrients, such as carbon or phosphorous, available in water, restricting bacterial growth (Hijnen et al. 2009, Vrouwenvelder et al. 2010). The third searches for a method by which bacterial adhesion onto virgin membranes can be mitigated. By using surface coatings or functional groups to alter the surface properties of membranes (Ba et al. 2010, Liu et al. 2010) it is thought that

the initial bacterial adhesion can be prevented, reducing the risk of biofilm development on the membrane's surface (Rana and Matsuura 2010). Mitigation of bacteria adhesion, however, requires a fundamental understanding of the complex mechanisms governing bacterial adhesion.

One of the complications to this preventative approach is the role of conditioning films on the membrane surface during bacterial adhesion. Despite pre-cleaning via coagulation and microfiltration, feed streams from fresh water sources will contain 1-3 mgC/L natural organic matter (Cyna et al. 2002, Ventresque et al. 2000). Within the first few seconds of exposure to the feed stream, a film of these organics a few molecules thick (Lorite et al. 2011) adsorbs on the membrane's surface which can have a significant impact on the surface's properties. Schneider showed the acid-base surface free energy components of conditioned hydrophilic and hydrophobic surfaces to be drastically different to the respective clean substrata (Schneider 1996). Conditioning films were also seen to have a strong influence on solid-liquid and solid-particle interfacial tensions as well as on the surface's free energy of particle adhesion.

A few studies have attempted to determine the influence of conditioning films on bacterial adhesion. Although the majority of these studies apply the Derjaguin-Landau-Verwey-Overbeek (DLVO) theory for predicting bacterial adhesion onto conditioned membranes, conflicting results have been reported from these investigations: in one set of studies, organic conditioning films were shown to increase the rate of bacterial adhesion (de Kerchove and Elimelech 2007, Hwang et al. 2012, Hwang et al. 2013), while other studies show the opposite for similar conditioning films (Garrido et al. 2014, Subramani et al. 2009). These opposing reports are due to the complexity of bacterial adhesion and the numerous differences between the experimental approaches taken. Feed composition, bacteria species, adhesion protocols (static or dynamic adhesion), cross-flow and permeation hydrodynamics,

as well as sample surface properties are all highly influential on bacterial adhesion and variable between studies (Habimana et al. 2014).

The inclusion of permeation hydrodynamics in some of the aforementioned studies might explain the observed large discrepancies in bacteria-membrane interactions. As additional molecules of the foulant deposit on the membrane surface (Tang et al. 2007), the film thickness will steadily grow over time resulting in the development of a thin fouling layer 10-50 μm thick as opposed to a conditioning film of a few molecules of thickness. The question then arises as to whether a thin fouling layer governs initial bacterial adhesion under permeation conditions in the same way as a conditioning film created by the initial adsorption of organic matter molecules does?

The objective of this study was to determine if thin organic fouling layers (less than 50 μm in thickness) govern initial bacterial adhesion in the same way as organic conditioning films (a few molecules thick) have been shown to, in an effort to explain previous conflicting results in the literature involving membrane conditioning during permeation. To achieve this, very thin fouling layers of humic acid (HA) and alginic acid (AA), two of the most predominant natural organic matter (NOM) foulants in fresh water filtration processes (Wilkinson et al. 1999), were created and the rate of initial adhesion of *Pseudomonas fluorescens* (a common bacteria species, abundant in soil) onto clean and HA- or AA- fouled NF membranes was quantified.

2. Materials & Methods

2.1. Pure Water

Laboratory water of the highest quality is imperative when conducting monoculture bacterial studies with membranes (Semiao et al. 2013). The water used throughout this project was Grade 1 pure water ($18.2 \text{ M}\Omega\cdot\text{cm}^{-1}$) obtained from an Elga Process Water System (Biopure 15 and Purelab flex 2, Veolia, Ireland), hereafter referred to as MilliQ water.

2.2. Model Foulants

Humic acid (HA; purchased as sodium salt, Sigma-Aldrich, Ireland) and Alginic Acid (AA; purchased as sodium salt, Sigma-Aldrich, Ireland) were used to represent typical fresh water organic foulants. HA was purified of ash content and smaller molecules by performing a series of precipitation-centrifugation steps followed by a week of dialysis and freeze-dried as described by Elimelech et al. (Hong and Elimelech 1997). It was not necessary to further purify AA.

Fouling solutions were made by dissolving HA (1 mgC/L) or AA (2 mgC/L) in 5 L of MilliQ water. To these solutions 20 mM sodium chloride (NaCl; Sigma-Aldrich, Ireland), 1 mM sodium bicarbonate (NaHCO_3 ; Sigma-Aldrich, Ireland) and 0.5 mM calcium chloride ($\text{CaCl}_2\cdot\text{H}_2\text{O}$; Merck, Ireland) were added to mimic freshwater. The organic foulants were fully dissolved prior to salt addition to avoid calcium complex formation. The salt control used in this study was prepared with the same salt concentrations in MilliQ water without organics.

For confocal microscopy studies, 1 mg of DAPI (2-(4-amidinophenyl)-1H-indole-6-carboxamide; Sigma-Aldrich, Ireland) was added as a fluorescent staining agent to the 5 L

of AA solution (final concentration 0.2 µg/ml). This solution was kept protected from the light throughout preparation and experimentation. No staining agent was required for the naturally fluorescent HA solution.

2.3. Filtration Membrane

The membranes used in this study were flat sheet TFC polyamide NF90 membranes (Dow Filmtec, USA) received as a single flat sheet roll. At equilibrium, membrane samples had a permeate flux rate of $8.7 \pm 0.6 \text{ L m}^{-2} \text{ hr}^{-1} \text{ bar}^{-1}$ and retained $91 \pm 1.5 \%$ of CaCl_2 and NaCl salts in the feed solution at 8 bar and 20°C.

Prior to experimentation, 27 cm x 5 cm rectangular samples were cut from the flat-sheet roll and soaked in MilliQ water overnight at 4°C to remove their preservative layer. They were subsequently soaked in 30% vol/vol Emsure® absolute ethanol (Merck, Ireland) in MilliQ water for 1.5 hours to disinfect them (Heffernan et al. 2013). The membranes were finally rinsed thoroughly to remove all traces of ethanol.

2.4. Model Bacterial Strain and Cell Preparation

Fluorescent mCherry-expressing *Pseudomonas fluorescens* PCL1701 (Lagendijk et al. 2010) was selected as the model strain in this study. *Pseudomonas* cultures were stored at -80°C in King B broth (King et al. 1954) supplemented with 20% glycerol. Cultured *Pseudomonas fluorescens* were obtained by inoculating 100 mL King B broth supplemented with gentamicin at a final concentration of 10 µg/mL using single colonies previously grown on King B agar (Sigma-Aldrich, Ireland) at 28°C. Subsequently, cultures were incubated overnight at 30°C with shaking at 100 rpm and left to grow to late exponential growth stages, corresponding to an Optical Density (OD_{600}) of 1.0.

For the study of bacterial adhesion onto NOM-fouled NF90 membranes, *Pseudomonas* cell suspensions were standardized by diluting overnight cultures to a final OD_{600} of 0.2 in 200 mL of a 0.1 M NaCl (Sigma-Aldrich, Ireland) solution. This ensured a standardized inoculum of approximately 10^8 cells/mL. Cells were then harvested by centrifugation at 5000 rpm for 10 min using a Sorval RC5C Plus centrifuge (Unitech, Ireland) and a Fiberlite™ f10-6x500y fixed angle rotor (Thermo Fisher Scientific Inc., Dublin, Ireland). The supernatant was carefully discarded and the pellet re-suspended in a portion of the feed solution using a vortex shaker (Stuart®, Mason technology, Dublin, Ireland).

2.5. Filtration Setup

Filtration experiments were performed using a cross-flow system (Figure 1) comprising of three Membrane Fouling Simulators (MFSs) (Vrouwenvelder et al. 2008) operated in parallel with an active filtration area of 0.008 m^2 each. The system operated in full recirculation mode using a high pressure pump (model P200, Hydra-Cell, UK). Two autoclavable feed tanks (Nalgene, VWR Ireland) were incorporated in the system, with one active at any time and valves in place to allow for switching between tanks without disturbing the flow or system pressure.

The pressure on the permeate side of the membranes was maintained at atmospheric pressure while the pressure on the feed side was controlled with a back-pressure regulator (KPB1L0A415P20000, Swagelok, UK) and monitored with two pressure transducers (PTX 7500, Druck, Radionics, Ireland) on the feed and retentate lines. The feed flow rate was measured using a flowmeter (OG2, Nixon flowmeters, UK) and maintained at 0.66 L/min through each MFS yielding a cross-flow rate of 0.39 m/s. The temperature of the active feed

tank was kept constant ($20 \pm 1^\circ\text{C}$) using a Julabo FP50 temperature control bath and a cooling coil. Temperature, flow rate and pressure measurements were recorded with a data-logger (Picolog 1000, PicoTechnology, Radionics, Ireland). Permeate flux measurements of each membrane were calculated by measuring the mass of liquid permeating each membrane in one minute. Permeate samples were obtained via the sample ports and feed samples were taken directly from the feed tank. Samples were not returned to the system after measurement.

2.6. Filtration System Cleaning Protocol

Prior to all filtration experiments the system was thoroughly cleaned. Feed tanks were routinely autoclaved at 120°C , scrubbed with bleach and rinsed repeatedly with MilliQ water to remove any adhered residual cells within the tanks' internal walls. The system was cleaned without a membrane by circulating lab grade IMS (Lennox Laboratory Supplies, Ireland) for one hour, and 0.1 M NaOH for two hours to remove bacteria and traces of the model foulants. The system was rinsed with MilliQ water after each phase of the cleaning regime. The pH of the system was adjusted to 7 by dropwise addition of 5 M HCL or 1 M NaOH over a two hour period, and then finally rinsed with MilliQ water. An additional one hour circulation of 20 mM EDTA (VWR, Ireland) was performed prior to IMS circulation in experiments subsequent to those using AA to remove traces of TEPs within the system.

2.7. Membrane Fouling

MilliQ water was filtered overnight with a transmembrane pressure of 15 bar to compact the NF90 membranes and obtain a steady pure-water flux. The feed was then switched via valves to a tank containing the selected fouling solution or salt control solution, without disrupting the flow. The system pressure was adjusted to 8 ± 0.5 bar for each solution to give a permeate

flux of $42 \text{ L.m}^{-2}.\text{hr}^{-1}$ (LMH) from each of the three MFSs. Filtration occurred for 3 hours with the three MFSs in parallel, during which minimal change to the pressure was required to keep the permeate flux constant for each fouling solution despite the development of fouling layers. Samples were taken hourly to monitor and maintain a constant feed conductivity ($2.6 \pm 0.05 \text{ mS/cm}$) and pH (8.5 ± 0.5), and to analyse membrane salt retention in the feed and permeate.

Once the fouling step was finished, one of the fouled MFS devices was removed from the cross-flow system in order to carry out fouling layer characterisation as described in the next sections. The other two MFS devices were left in the cross-flow system in order to carry out the bacterial adhesion experiments. The removed MFS was opened whilst submerged in MilliQ water to preserve the integrity of the fouling layer, and the fouled membrane was removed. For confocal studies three samples were cut from specific locations (inlet, mid-section and outlet) and placed in individual wells of a Lab-Tek® Chamber Slide™ 4-well system (Nunc®; ThermoScientific, Dublin, Ireland) previously filled with MilliQ water. Further samples were taken for fouling layer characterisation via Contact Angle and Zeta Potential. These samples were laid in petri dishes and left to dry in ambient conditions (covered to avoid air particle deposition). A sample for AFM was also taken and submerged in a petri dish of MilliQ water.

2.8. Adhesion Experiment and Quantification

After the removal of one MFS from the cross-flow system, as described above, the feed flow rate was adjusted to maintain a cross-flow velocity of 0.66 L/min ($\text{Re} = 548$) in each MFS in order to keep the same hydrodynamic conditions as the ones used during the fouling step. A bacterial inoculum containing approximately 10^8 cells/mL was added to the fouling solution

in the feed tank and recirculated in the system for 30 minutes at the same constant filtration conditions as the ones used during fouling. Permeate flux and conductivity measurements for each membrane cell and a measurement of the feed's conductivity were taken every ten minutes. Every experiment (i.e. fouling step + fouling characterisation + bacterial adhesion) was repeated at least twice to ensure reproducibility.

The two MFS cells were separated from the system at the end of the bacterial adhesion experiments, and carefully opened whilst submerged in MilliQ water in order to preserve the integrity of the fouling layer. The fouled membranes were removed, three pieces cut from different locations (inlet, mid-section and outlet) of the membrane and each sample was placed at the bottom of small petri dishes submerged in MilliQ water. Bacterial cells adhered to the fouled membranes were then observed under an epi-fluorescence microscope (Olympus BX51) using a 10X objective. Fluorescent mCherry-tagged *Pseudomonas* cells were detected using the microscope's U-MNG or U-MWIB excitation/emission filter cubes systems. Ten micrographs were obtained at random points from each membrane sample. Cell surface coverage (%) was then determined, from grayscaled and thresholded acquired images for each membrane using ImageJ® software, a Java-based image processing program (<http://rsbweb.nih.gov/ij/>). At the concentration used, the HA layer's natural fluorescence did not interfere with mCherry fluorescence signals.

2.9. Structural Analysis of Fouled Membranes

To assess the organic fouling layers on the membranes, horizontal-plane images of fouled membrane samples in their Lab-Tec® wells were acquired using an Olympus Fluoview FV 1000 Confocal microscope.

The excitation wavelength used for detecting DAPI-stained SA was 405 nm, and emitted fluorescence was recorded within the range of 420 to 460 nm (Lee et al. 2011). For HA conditioned membranes, an excitation wavelength of 488 nm and auto-fluorescence was recorded at 500-550 nm. Images (1269 μm x 1269 μm) were collected through a UPLSAPO 10x objective (numerical aperture NA 0.4) with a z-step of 1 μm . 3D projections were performed with Zen software (Zeiss). The structural quantification of the NOM conditioning layer (biovolume, surface coverage, thickness and roughness) was performed using the PHLIP Matlab program developed by J. Xavier (<http://sourceforge.net/projects/phlip/>)(Mueller et al. 2006).

2.10. Surface Properties of Fouled Membranes

The Lifshitz-van der Waals (γ_{LW}), electron-donor (γ^-) and electron-acceptor (γ^+) surface tension components of dehydrated treated NF90 membrane samples (S) were determined by measuring contact angles using the following expression:

$$\cos\theta = -1 + 2 \left(\gamma_{\text{S}}^{\text{LW}} \gamma_{\text{L}}^{\text{LW}} \right)^{\frac{1}{2}} / \gamma_{\text{L}} + 2 \left(\gamma_{\text{S}}^+ \gamma_{\text{L}}^- \right)^{\frac{1}{2}} / \gamma_{\text{L}} + 2 \left(\gamma_{\text{S}}^- \gamma_{\text{L}}^+ \right)^{\frac{1}{2}} / \gamma_{\text{L}} \quad (1)$$

Contact angles (θ) and surface energy measurements (γ_{S}) of dehydrated compacted NF90 membrane were measured at room temperature using a goniometer (OCA 20 from Dataphysics Instruments) with three static pure liquids (L): deionised water, diiodomethane and ethylene glycol.

The Lewis acid-base component was deduced from:

$$\gamma_{\text{S}}^{\text{AB}} = 2\sqrt{(\gamma_{\text{S}}^+ \gamma_{\text{S}}^-)} \quad (2)$$

And the total surface energy was defined by:

$$\gamma_{\text{S}} = \gamma_{\text{S}}^{\text{AB}} + \gamma_{\text{S}}^{\text{LW}} \quad (3)$$

The interfacial free energy of adhesion (ΔG_{132}) was calculated from these derived components using the method laid out by Brant and Childress (Brant and Childress 2002).

Values for bacterial surface components were taken from a study on *Pseudomonas fluorescens* by Smets et al.: $\gamma^- = 34.9 \text{ mJ/m}^2$, $\gamma^+ = 0.22 \text{ mJ/m}^2$, and $\gamma^{\text{LW}} = 30.8 \text{ mJ/m}^2$ (Smets et al. 1999).

Samples for zeta potential analysis were dried in air overnight, rehydrated in MilliQ water for an hour and then submerged in a 5 mM NaCl solution overnight as described previously by Elimelech (Xie et al. 2013). There was a slight dissolution of the fouling layer upon introduction into the salt solution but it was greatly minimised by the dehydration-rehydration step. Streaming potential measurements of the fouled membranes were conducted using a ZetaCad system (CAD instruments, France) with a 5 mM NaCl (pH 8, 0.5 mS/cm) solution streamed through a 150 μm channel between two similarly fouled samples. By varying the flow rate through the channel and measuring the voltage difference across the chamber the zeta potential was calculated.

2.11. Atomic Force Microscopy

Surface layer stiffness and adhesive properties of fouled and clean membranes were characterised by analysing indentation and retraction curves obtained from AFM-based Force Spectroscopy measurements. Force measurements were performed using a JPK NanoWizard II BioAFM (JPK Instruments, Germany) integrated with an inverted optical microscope (Nikon, Japan) and a Hamamatsu CCD camera. This ensemble was enclosed in an acoustic isolation chamber, and placed on a vibration isolation table (TS-150, JRS Scientific Instruments, Switzerland).

A commercial silicon nitride cantilever with a sharp triangular silicon nitride tip of 60 nm radius (DNP-10, C type, Bruker, UK) was used in this study. The spring constant of the

cantilevers was calibrated as 0.142 N/m at the room temperature, using the thermal noise method. Force curves were measured while approaching within 0.5 μm from the salt control membrane's surface and while approaching and penetrating the top 0.5 - 1 μm of the created AA and HA fouling layers. The area between the two force curves for each sample was calculated computationally. In each case this area was subdivided into two areas by the horizontal line representing 0 N, the area above this line was recorded as the 'energy dissipated in approach' while the area below it was recorded as the 'energy dissipated in retraction'. For comparative reasons these area values were divided by the width of the curves (distance travelled by the tip) to correct the values to a full 1 μm .

After several force curve measurements, several force curves were recorded on a clean surface (i.e. glass) in order to observe the possible residual forces on the retraction curves due to the tip contamination. When contaminated, the cantilever was carefully rinsed with ethanol and Milli-Q water, before being placed in UV Ozone cleaner (ProCleaner, Bioforce Nanosciences, USA). Force curves were collected at a velocity of 2 $\mu\text{m/s}$ up to a force set-point limit of 18 nN.

3. Results & Discussion

3.1. Surface Characterisation of the Fouling layer

Images taken with the confocal microscope were combined to create image stacks from which the density, height and roughness of the created fouling layers were determined at three locations along the length of the flow channel (Figure 2).

The AA fouling layers created had an average thickness of $25 \pm 4 \mu\text{m}$ and a surface coverage higher than 70% along the length of the membrane. This layer was very reproducible with less than 20% difference between fouling layers created for most parameters. The largest

variations were seen in the roughness measurements which may be associated with AA's tendency to bind with calcium to create clumps (Listiarini et al. 2009).

The HA fouling layer in contrast shows an increase in thickness in the middle section of the membrane; the fouling layer bulges by 66% from $20 \pm 4 \mu\text{m}$ at the inlet to a maximum of $34 \pm 8 \mu\text{m}$ before returning to a thickness of $25 \pm 7 \mu\text{m}$ at the outlet. This bulge is accompanied with a 20% drop in surface coverage and a steady rise in roughness along the length of the flow channel. It appears that HA deposits as a thin even layer at the inlet of the channel, becoming rougher and less evenly dispersed for the midsection and the outlet. This trend was evident in each of the membrane samples studied. The largest variations between experiments were again in the roughness measurements, especially at the outlet of the MFS.

The average roughness of each fouling layer was calculated by multiplying the layer thickness by the Fouling Layer Roughness factor presented in Figure 2d (Heydorn et al. 2000). The AA layer has an average roughness along the length of the membrane of $5.3 \pm 0.7 \text{ nm}$ while the HA layer increases along the membrane length, from 2.3 nm at the inlet to 9.4 nm at the outlet. These values are smoother than the values reported for a clean NF90 membrane which has an average roughness of 60 nm (Xu et al. 2006).

The surface coverage and thickness measurements of the independent experiments show that the fouling layers created under the same fouling conditions are reproducible. The small variances between the layers may be associated with the large range of molecule sizes in each substance or with the heterogeneous nature of the membrane surface which can lead to flux hotspots (Ramon and Hoek 2013). Errors may also have occurred due to slight dissociation of

the fouling layer upon exposure to MilliQ water when the samples were transferred from the MFS to the confocal sample chambers.

3.2. Surface Energy

Within 100 nm of a surface the forces dominating a single bacterial cell's movements will be the van der Waal's force, the Lewis acid-base interaction and repulsion from the electrostatic double-layer (Brant and Childress 2002).

Table 1: Measured zeta potential (ζ) and contact angle values, and derived electron acceptor (γ^+), electron donor (γ^-), Lifshitz van der Waals (γ^{LW}), Acid-base (γ^{AB}), total surface tension (γ^{total}) and total interfacial free energy of adhesion (ΔG_{132}) of the surface energies of NF90 membranes fouled with humic acid, alginic acid or with a salt control. Contact angle measurements and derived components of surface energy were taken from 20 measurements on two independent samples. The average values and standard errors values are shown.

	Salt Control	Humic Acid	Alginic Acid
Contact Angle ($^\circ$)	43.6 ± 2.75	43.5 ± 0.45	23.6 ± 0.5
γ^- (mJ/m ²)	43.0 ± 0.14	39.8 ± 0.4	38.0 ± 0.21
γ^+ (mJ/m ²)	0.06 ± 0.011	0.35 ± 0.045	0.18 ± 0.037
γ^{LW} (mJ/m ²)	40.13 ± 3.48	51.79 ± 1.03	72.38 ± 0.95
γ^{AB} (mJ/m ²)	2.88 ± 0.3	7.22 ± 0.53	4.77 ± 0.54
γ^{total} (mJ/m ²)	43.02 ± 3.42	59.01 ± 1.48	77.15 ± 1.41
ΔG_{132} (mJ/m ²)	19.1	14.7	11.38
ζ (mV)	-23.1 ± 0.71	-25.7 ± 0.007	-23.1 ± 1.23

The obtained results (Table 1) show that the addition of the HA fouling layer did not change the shape of a droplet compared to the droplet shape on the clean membrane. The addition of an AA layer, however, caused the membrane to become more hydrophilic with a reduction in contact angle from $43.6 \pm 2.75^\circ$ to $23.6 \pm 0.5^\circ$. To gain a better understanding of the forces involved a more expansive analysis was undertaken.

The derived components of surface energy reveal numerous changes that have occurred upon addition of the fouling layer. The apolar Lifshitz-van der Waals component has increased from $40.13 \pm 3.48 \text{ mJ/m}^2$ of the clean membrane to $51.79 \pm 1.48 \text{ mJ/m}^2$ and $72.38 \pm 0.95 \text{ mJ/m}^2$ for membranes fouled with HA and AA, respectively. The polar Lewis acid-base component was also higher for the two layers of fouling than for the clean membrane, but to a much lesser extent.

Calculations of the interfacial free energy of adhesion (ΔG_{132}) yielded lower resultant energies for HA and AA, 14.7 mJ/m^2 and 11.38 mJ/m^2 , respectively, than for the salt control membrane, with 19.1 mJ/m^2 . Lower energies of adhesion indicate less bacterial repulsion and therefore less resistance to adhesion (Subramani and Hoek 2008). This suggests that based on contact angle measurements, bacteria should adhere to the largest extent on the AA fouled membrane, to a lesser extent on the HA fouled membrane and to the lowest extent on the salt control, non-fouled membrane.

3.3. Zeta Potential

The addition of a fouling layer did not appear to significantly affect the zeta potential of the membrane (Table 1), hence not contributing to differences in bacterial adhesion. While the HA layer exhibited a statistically more negative zeta potential, in the context of a study by Li et al. (Li and Logan 2004) who correlated bacterial adhesion to zeta potential over the range 0 to - 60 mV, a difference of 2 mV is not expected to be great enough to have any appreciable effect on bacterial adhesion. There is a notable risk of error in these measurements, however. Fresh fouling layers subjected to the salt solution used in the streaming potential analysis tended to dissociate from the membrane. It was therefore necessary to allow the samples to

dry and re-soak the samples in MilliQ water prior to measurement, as has been shown in previous studies (Xie et al. 2013). This protocol leads to a compaction and re-expansion of the fouling layer; furthermore, it may also lead to leaching of certain salts from within the layer, which may have altered the zeta potential of the layer.

As the streaming potential measurements were taken with a liquid of different ionic strength than the fouling solution, the zeta potential values shown should not be used as a direct indication of bacterial adhesion; they are merely for comparative purposes.

3.4. Atomic Force Microscopy

AFM was employed to compare the physical properties of the fouling layers. Repulsive forces were measured when approaching the clean membrane samples and while penetrating into the top of the fouling layers, whilst adhesive forces were measured when retracting the probe from each sample (Figure 3) .

Approaching the clean membrane's surface required a small amount of energy (10^{-15} J/ μm) as the probe was repelled by the membrane's surface charge. With the addition of the fouling layers, however, the probe required a much larger magnitude of energy (10^{-7} J/ μm) per micron of movement. The probe in this case was still more than 20 μm away from the membrane's surface and thus would not have felt the membrane's repulsion; the energy dissipated is hence related to the resistance to penetration of the relatively dense fouling layer itself.

When the probe was retracted from the fouling layers there was a notable strain as the sticky fouling layers resisted the probe's removal. The 10^{-8} J/ μm required to escape the HA and AA

layers is once again many orders of magnitude higher than the 10^{-16} J/ μ m required to retract the probe from the salt control membrane.

On average the energy required to retract from the membrane or fouling layers was one order of magnitude lower than the energy required to approach or penetrate them. This agrees with the positive values of ΔG_{132} shown previously that suggested the overall charge on the membrane's surface (fouled and not fouled) would most likely repel bacteria. These results show a notable resistance to penetration and escape from a fouled membrane that is not present for the salt control. This suggests that the layers may act as an obstacle resisting bacterial penetration leading to a lower rate of bacterial adhesion onto the NF membrane surface.

On average more energy was dissipated when penetrating the HA layer (2.33×10^{-7} J/ μ m) than the AA layer (1.32×10^{-7} J/ μ m). The reverse was true when retracting the probe which exhibited a higher average dissipation of energy moving through the AA layer (3.3×10^{-8} J/ μ m) than the HA layer (1.18×10^{-8} J/ μ m). These results would therefore suggest that bacterial adhesion would occur to a greater extent within the AA layer, as it is more likely that bacterial cells would penetrate the layer and less likely that they would be able to escape it. These differences are, however, of a much smaller magnitude than those described previously between fouled and clean NF90 membranes.

3.5. Bacterial Adhesion onto Fouled Membranes

A previous study showed that in the presence of a thin conditioning film of organic compounds on a surface (a few molecules of thickness), bacterial cells deposited on top of the film (Hwang et al. 2013). In contrast, microscopic analysis of bacterial adhesion onto organic fouled NF90 membranes under permeate flux conditions showed this was not the case. All of

the bacteria were seen to penetrate the HA and AA fouling layers and adhere directly to the NF90 membrane's surface. No bacteria were seen on top of the organic fouling layer or suspended within it. The surface coverage values shown in Figure 4 are hence representative of the bacteria adhered at the membrane's surface level, within the fouling layer in the case of HA and AA.

Despite indications from the surface energy measurements that the fouling layers would promote bacterial adhesion, the results of microscopic studies show considerably greater numbers of bacteria adhering to the unfouled salt control membrane (Figure 4). This suggests that the forces measured via AFM are a more accurate indicator of the extent of bacterial adhesion under permeate flux onto thinly organic fouled membranes than those measured via surface energy studies, the most commonly used technique to characterise conditioning film layers and explain bacterial adhesion (Hwang et al. 2013, Subramani et al. 2009).

Of the two fouling layers, HA is slightly more prone to bacterial adhesion ($t(78) = 4.3$, $p < 0.001$; $9.8 \pm 4\%$ surface coverage) than the AA layer ($7.5 \pm 4\%$ surface coverage) as can be seen in Figure 4, while contact angle measurements indicated that bacterial adhesion was expected to occur mainly in the AA fouling layer. Despite AFM results also indicating a more prone adhesion to AA fouling layers compared to HA layers, the differences expected were very small ($1.32 \times 10^{-7} \text{ J}/\mu\text{m}$ and $2.33 \times 10^{-7} \text{ J}/\mu\text{m}$, respectively). The difference of bacterial adhesion between the two types of fouling layers tested is however only one sixth of the difference between fouled and clean membranes.

Rougher membrane surfaces have been shown to have a higher propensity for bacterial adhesion as the heterogeneity of the surface yields rough features which are more favourable

sites for surface-bacteria bonding (Subramani and Hoek 2008). There is a positive correlation between cell surface coverage and average surface roughness for clean and fouled NF90 membranes in this experiment. However the bacteria did not bond directly to the surface of the fouling layers, hence a correlation between adhesion and surface roughness would be misleading, as will be discussed in the next section.

Subramani and Hoek discussed the forces acting upon bacteria in their 2008 study with clean NF and RO membranes (Subramani and Hoek 2008). They described six forces which dominate bacteria adhesion in cross-flow configuration. These are: cross-flow lift (F_{CL}), permeate drag (F_{PD}), gravity (F_G), Lifshitz-van der Waal's force (F_{LW}), electrostatic double layer (F_{EL}), and acid base force (F_{AB}). At a distance greater than 100 nm from the membrane's surface the first three of these forces dominate bacterial movement. If the drag due to the permeating liquid is strong enough to counteract the lifting force associated with cross-flow, the bacteria will be drawn towards the membrane surface. Once the bacteria are within 100 nm of the membrane's surface their movement is subjected also to the short range forces such as Lifshitz-van der Waal's forces. If the additional attraction of the Lifshitz-van der Waal's force is enough to overcome the repulsion of the electrostatic double layer and the acid base interactions, the bacteria is likely to attach to the membrane (assuming both membrane and bacteria are negatively charged as is the case for this study).

Correlations between bacterial adhesion and hydrophobicity, or with other membrane surface energy properties, assume that bacteria have an equal probability of approaching within a distance of 100 nm from the surface of the membrane. This is an acceptable assumption for clean membranes or for studies of conditioning films, which are no more than a few nanometres thick. For fouling layers thicker than 100nm, however, bacteria first interact with

the fouling layer outside this 100 nm region. The additional physical force required to penetrate the fouling layer has a greater influence on bacterial transport than the surface energy effects, as shown above where fouling layers of different surface properties but similar thickness were subject to similar amounts of bacterial adhesion. The permeate drag force must now overcome the fouling layer's resistance as well as the cross-flow lift in order for bacteria to reach a proximity to the membrane surface whereby short range surface energy forces can take effect. In this case surface energy effects of the fouling layer of the membrane surface alone cannot be used to analyse bacterial adhesion through fouling layers thicker than 100 nm.

3.6. Bacterial Adhesion Profile Along the Length of the Membrane

Microscopic analysis of the fouled membranes showed a significant change in the number of bacteria adhered onto different sections along the length of the membrane. Despite the heterogeneous nature of NF membranes, the average surface properties on a micron scale should not change along the length of the membrane surface. Similarly, with an average bacteria count of 10^7 cells/mL in the feed tank, the feed solution flowing across the membrane surface should not change significantly in bacterial concentration along the length of the channel. It is therefore unexpected that bacteria would adhere to different extents at the inlet, mid-section and outlet.

One of the six forces mentioned previously will however change along the channel length. As water permeates the initial sections of the membrane the pressure within the channel slightly drops leading to a lower driving force for permeation and thus lower permeate drag forces in subsequent stages of the channel (Geissler and Werner 1995). This permeate drag gradient

could result in a gradient in initial bacterial adhesion, with a high concentration of bacteria at the inlet and a lower adhesion at the outlet.

Furthermore, Busscher and van der Mei described a pseudo-end phase to initial bacterial deposition whereby adhesion slows down due to inter-bacterial blocking (Busscher and van der Mei 2006) caused by the repulsion effect of bacteria adhered to the membrane. Bacterial cells approaching a densely populated membrane surface are likely to be repelled, adhering instead downstream to a more sparsely populated region. In this way an even lawn of bacterial cells eventually develops across the membrane surface.

This is seen for the salt control membrane which had an even 24 ± 3 % surface coverage of bacteria on each section of the membrane (Figure 5). This is indicative that within the 30 minutes of adhesion the system reached the pseudo-end stage. For the fouled membranes, however, a significant reduction in bacterial adhesion was seen along the membrane channel, indicating that a pseudo-end stage was not reached.

Adhesion through the HA layer fell from 15.2 ± 2 % bacterial surface coverage at the inlet to 7.3 ± 2 % and 7.0 ± 2 % in the mid-section and outlet, respectively. A lesser reduction was seen for adhesion through the AA layer: 11.4 ± 4.5 % (inlet), 6.5 ± 2.4 % (mid-section) and 4.5 ± 1.2 % (outlet). These reductions on the latter stages of the fouled membranes do not correlate with any of the trends in membrane properties quantified with the confocal microscope (Figure 2). The reducing trend in adhesion to the HA fouled NF90 membrane directly contrasts with the increasing trend in HA surface roughness (Figure 2 d): roughness is therefore not a dominant factor during bacterial adhesion onto organic fouled NF membranes. The same applies to AA: despite the AA roughness not changing along the

membrane length, bacterial adhesion decreases substantially from the inlet ($11.4 \pm 4.5 \%$) to the outlet ($4.5 \pm 1.2 \%$). This bacterial adhesion trend is instead indicative of the permeate drag force gradient along the channel length.

Bacteria in the initial sections of the membrane are subjected to the strongest permeate drag force and thus are most likely to overcome the penetration resistances of the fouling layers measured by the AFM. In the latter sections of the channel however the lower drag forces result in fewer bacteria penetrating the fouling layers.

As was the case with the AFM results, the differences in adhesion between the fouling layers for each section are insignificant compared to the differences between fouled and non-fouled membranes. With a maximum surface coverage of 15%, adhesion onto the fouled membranes has not reached the pseudo-end stage seen with the non-fouled membranes ($24 \pm 3\%$ surface coverage along the entire membrane). The uneven distribution of bacteria along the channel length may therefore be due to absence of inter-bacterial blocking across the membrane surface.

4. Conclusion

Fouling layers of Humic Acid and Alginic Acid between 20 and 35 μm thick were shown to decrease bacterial adhesion in cross-flow filtration under permeate flux conditions. The opposite trend would be expected based on surface energy results obtained from contact angle measurements of the fouling layer deposited on the membrane surface and assuming the bacteria would adhere on the fouling layer surface. All adhered bacterial cells were instead seen to adhere directly onto the membrane surface in all experiments and were not entrained in the fouling layers. AFM proved to be a useful tool in this study as it showed that

bacteria require a much greater magnitude of energy to reach the membrane's surface when penetrating the NOM fouling layers.

This study has shown that bacterial adhesion in the presence of a fouling layer and permeate flux to be notably different from conditioning film experiments in which bacteria adhere onto an ultrathin conditioning layer. It is imperative that future studies of bacterial adhesion onto conditioning films or fouling layers under permeate flux conditions are aware of this difference and monitor the created layer's thickness to avoid potential errors arising from layer resistance.

Further research in this area is required to study the impact of this decreased adhesion on biofouling development in the absence and presence of an organic matter fouling layer and for different environmental conditions such as the presence or absence of nutrients.

5. Acknowledgements

This research was supported by the European Research Council (ERC), project 278530, funded under the EU Framework Programme 7 and also with the financial support of Science Foundation Ireland under Grant Number "SFI 11/RFP.1/ENM/3145. The authors would like to thank Mr. Pat O'Halloran for his invaluable technical assistance, and Mr. Liam Morris for the construction of the MFS devices. The authors especially thank Dr. Ellen L. Lagendijk from the Institute of Biology Leiden, Netherlands for the gift of the *Pseudomonas fluorescens* WCS365, PCL1701

614 6. References

- 615 Ba, C., Ladner, D.A. and Economy, J. (2010) Using polyelectrolyte coatings to improve
616 fouling resistance of a positively charged nanofiltration membrane. *Journal of Membrane*
617 *Science* 347(1–2), 250-259.
- 618 Brant, J.A. and Childress, A.E. (2002) Assessing short-range membrane–colloid interactions
619 using surface energetics. *Journal of Membrane Science* 203(1–2), 257-273.
- 620 Busscher, H.J. and van der Mei, H.C. (2006) Microbial adhesion in flow displacement
621 systems. *Clinical microbiology reviews* 19(1), 127-141.
- 622 Chen, X. and Stewart, P.S. (2000) Biofilm removal caused by chemical treatments. *Water*
623 *Research* 34(17), 4229-4233.
- 624 Cyna, B., Chagneau, G., Bablon, G. and Tanghe, N. (2002) Two years of nanofiltration at the
625 Méry-sur-Oise plant, France. *Desalination* 147(1–3), 69-75.
- 626 de Kerchove, A.J. and Elimelech, M. (2007) Impact of alginate conditioning film on
627 deposition kinetics of motile and nonmotile *Pseudomonas aeruginosa* strains. *Applied and*
628 *Environmental Microbiology* 73(16), 5227-5234.
- 629 Flemming, H.-C. (1997) Reverse osmosis membrane biofouling. *Experimental Thermal and*
630 *Fluid Science* 14(4), 382-391.
- 631 Garrido, K.D., Palacios, R.J.S., Lee, C. and Kang, S. (2014) Impact of conditioning film on
632 the initial adhesion of *E. coli* on polysulfone ultrafiltration membrane. *Journal of Industrial*
633 *and Engineering Chemistry* 20(4), 1438-1443.
- 634 Geissler, S. and Werner, U. (1995) Dynamic model of crossflow microfiltration in flat-
635 channel systems under laminar flow conditions. *Filtration & Separation* 32(6), 533-537.
- 636 Habimana, O., Semiao, A.J.C. and Casey, E. (2014) The role of cell-surface interactions in
637 bacterial initial adhesion and consequent biofilm formation on nanofiltration/reverse osmosis
638 membranes. *Journal of Membrane Science* 454, 82-96.
- 639 Heffernan, R., Semião, A.J.C., Desmond, P., Cao, H., Safari, A., Habimana, O. and Casey, E.
640 (2013) Disinfection of a polyamide nanofiltration membrane using ethanol. *Journal of*
641 *Membrane Science* 448(0), 170-179.
- 642 Heydorn, A., Nielsen, A.T., Hentzer, M., Sternberg, C., Givskov, M., Ersbøll, B.K. and
643 Molin, S. (2000) Quantification of biofilm structures by the novel computer program
644 COMSTAT. *Microbiology* 146(10), 2395-2407.
- 645 Hijnen, W.A.M., Biraud, D., Cornelissen, E.R. and van der Kooij, D. (2009) Threshold
646 Concentration of Easily Assimilable Organic Carbon in Feedwater for Biofouling of Spiral-
647 Wound Membranes. *Environmental Science & Technology* 43(13), 4890-4895.
- 648 Hong, S. and Elimelech, M. (1997) Chemical and physical aspects of natural organic matter
649 (NOM) fouling of nanofiltration membranes. *Journal of Membrane Science* 132(2), 159-181.
- 650 Hwang, G., Kang, S., El-Din, M.G. and Liu, Y. (2012) Impact of conditioning films on the
651 initial adhesion of *Burkholderia cepacia*. *Colloids and Surfaces B: Biointerfaces* 91(0), 181-
652 188.
- 653 Hwang, G., Liang, J., Kang, S., Tong, M. and Liu, Y. (2013) The role of conditioning film
654 formation in *Pseudomonas aeruginosa* PAO1 adhesion to inert surfaces in aquatic
655 environments. *Biochemical Engineering Journal* 76(0), 90-98.
- 656 King, E.O., Ward, M.K. and Raney, D.E. (1954) Two Simple Media for the Demonstration of
657 Pyocyanin and Fluorescin. *Journal of Laboratory and Clinical Medicine* 44(2), 301-307.
- 658 Lagendijk, E.L., Validov, S., Lamers, G.E.M., de Weert, S. and Bloemberg, G.V. (2010)
659 Genetic tools for tagging Gram-negative bacteria with mCherry for visualization in vitro and
660 in natural habitats, biofilm and pathogenicity studies. *Fems Microbiology Letters* 305(1), 81-
661 90.

Lee, Y.-H., Chang, J.-J., Lai, W.-F., Yang, M.-C. and Chien, C.-T. (2011) Layered hydrogel of poly (γ -glutamic acid), sodium alginate, and chitosan: Fluorescence observation of structure and cytocompatibility. *Colloids and Surfaces B: Biointerfaces* 86(2), 409-413.

Li, B. and Logan, B.E. (2004) Bacterial adhesion to glass and metal-oxide surfaces. *Colloids and Surfaces B: Biointerfaces* 36(2), 81-90.

Liikanen, R., Yli-Kuivila, J. and Laukkanen, R. (2002) Efficiency of various chemical cleanings for nanofiltration membrane fouled by conventionally-treated surface water. *Journal of Membrane Science* 195(2), 265-276.

Listiari, K., Chun, W., Sun, D.D. and Leckie, J.O. (2009) Fouling mechanism and resistance analyses of systems containing sodium alginate, calcium, alum and their combination in dead-end fouling of nanofiltration membranes. *Journal of Membrane Science* 344(1-2), 244-251.

Liu, C.X., Zhang, D.R., He, Y., Zhao, X.S. and Bai, R. (2010) Modification of membrane surface for anti-biofouling performance: Effect of anti-adhesion and anti-bacteria approaches. *Journal of Membrane Science* 346(1), 121-130.

Lorite, G.S., Rodrigues, C.M., de Souza, A.A., Kranz, C., Mizaikoff, B. and Cotta, M.A. (2011) The role of conditioning film formation and surface chemical changes on *Xylella fastidiosa* adhesion and biofilm evolution. *Journal of Colloid and Interface Science* 359(1), 289-295.

Mueller, L.N., De Brouwer, J.F., Almeida, J.S., Stal, L.J. and Xavier, J.B. (2006) Analysis of a marine phototrophic biofilm by confocal laser scanning microscopy using the new image quantification software PHLIP. *BMC ecology* 6(1), 1.

Ramon, G.Z. and Hoek, E.M.V. (2013) Transport through composite membranes, part 2: Impacts of roughness on permeability and fouling. *Journal of Membrane Science* 425-426(0), 141-148.

Rana, D. and Matsuura, T. (2010) Surface modifications for antifouling membranes. *Chemical Reviews* 110(4), 2448-2471.

Schneider, R.P. (1996) Conditioning Film-Induced Modification of Substratum Physicochemistry—Analysis by Contact Angles. *Journal of Colloid and Interface Science* 182(1), 204-213.

Semiao, A.J.C., Habimana, O., Cao, H., Heffernan, R., Safari, A. and Casey, E. (2013) The importance of laboratory water quality for studying initial bacterial adhesion during NF filtration processes. *Water Research* 47(8), 2909-2920.

Smets, B.F., Grasso, D., Engwall, M.A. and Machinist, B.J. (1999) Surface physicochemical properties of *Pseudomonas fluorescens* and impact on adhesion and transport through porous media. *Colloids and Surfaces B: Biointerfaces* 14(1-4), 121-139.

Subramani, A. and Hoek, E.M.V. (2008) Direct observation of initial microbial deposition onto reverse osmosis and nanofiltration membranes. *Journal of Membrane Science* 319(1-2), 111-125.

Subramani, A., Huang, X. and Hoek, E.M.V. (2009) Direct observation of bacterial deposition onto clean and organic-fouled polyamide membranes. *Journal of Colloid and Interface Science* 336(1), 13-20.

Tang, C.Y., Kwon, Y.-N. and Leckie, J.O. (2007) Characterization of humic acid fouled reverse osmosis and nanofiltration membranes by transmission electron microscopy and streaming potential measurements. *Environmental Science & Technology* 41(3), 942-949.

Ventresque, C., Gisclon, V., Bablon, G. and Chagneau, G. (2000) An outstanding feat of modern technology: the Mery-sur-Oise nanofiltration Treatment plant (340,000 m³/d). *Desalination* 131(1-3), 1-16.

Vrouwenvelder, J.S., Beyer, F., Dahmani, K., Hasan, N., Galjaard, G., Kruithof, J.C. and Van Loosdrecht, M.C.M. (2010) Phosphate limitation to control biofouling. *Water Research* 44(11), 3454-3466.

Vrouwenvelder, J.S., Manolarakis, S.A., van der Hoek, J.P., van Paassen, J.A.M., van der Meer, W.G.J., van Agtmaal, J.M.C., Prummel, H.D.M., Kruithof, J.C. and van Loosdrecht, M.C.M. (2008) Quantitative biofouling diagnosis in full scale nanofiltration and reverse osmosis installations. *Water Research* 42(19), 4856-4868.

Wilkinson, K.J., Balnois, E., Leppard, G.G. and Buffle, J. (1999) Characteristic features of the major components of freshwater colloidal organic matter revealed by transmission electron and atomic force microscopy. *Colloids and Surfaces A: Physicochemical and Engineering Aspects* 155(2-3), 287-310.

Xie, M., Nghiem, L.D., Price, W.E. and Elimelech, M. (2013) Impact of humic acid fouling on membrane performance and transport of pharmaceutically active compounds in forward osmosis. *Water Research* 47(13), 4567-4575.

Xu, P., Drewes, J.E., Kim, T.-U., Bellona, C. and Amy, G. (2006) Effect of membrane fouling on transport of organic contaminants in NF/RO membrane applications. *Journal of Membrane Science* 279(1-2), 165-175.

Yuan, Y. and Kilduff, J.E. (2010) Effect of colloids on salt transport in crossflow nanofiltration. *Journal of Membrane Science* 346(2), 240-249.

Figures

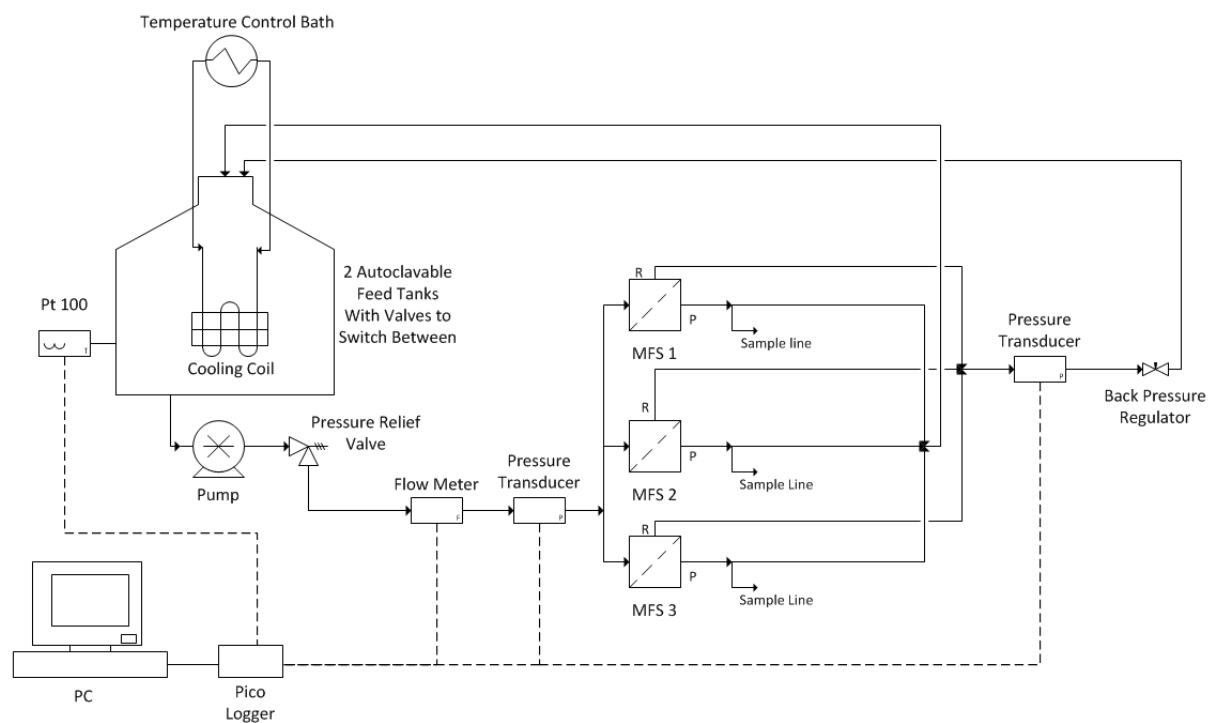


Figure 1: Crossflow Filtration System Setup

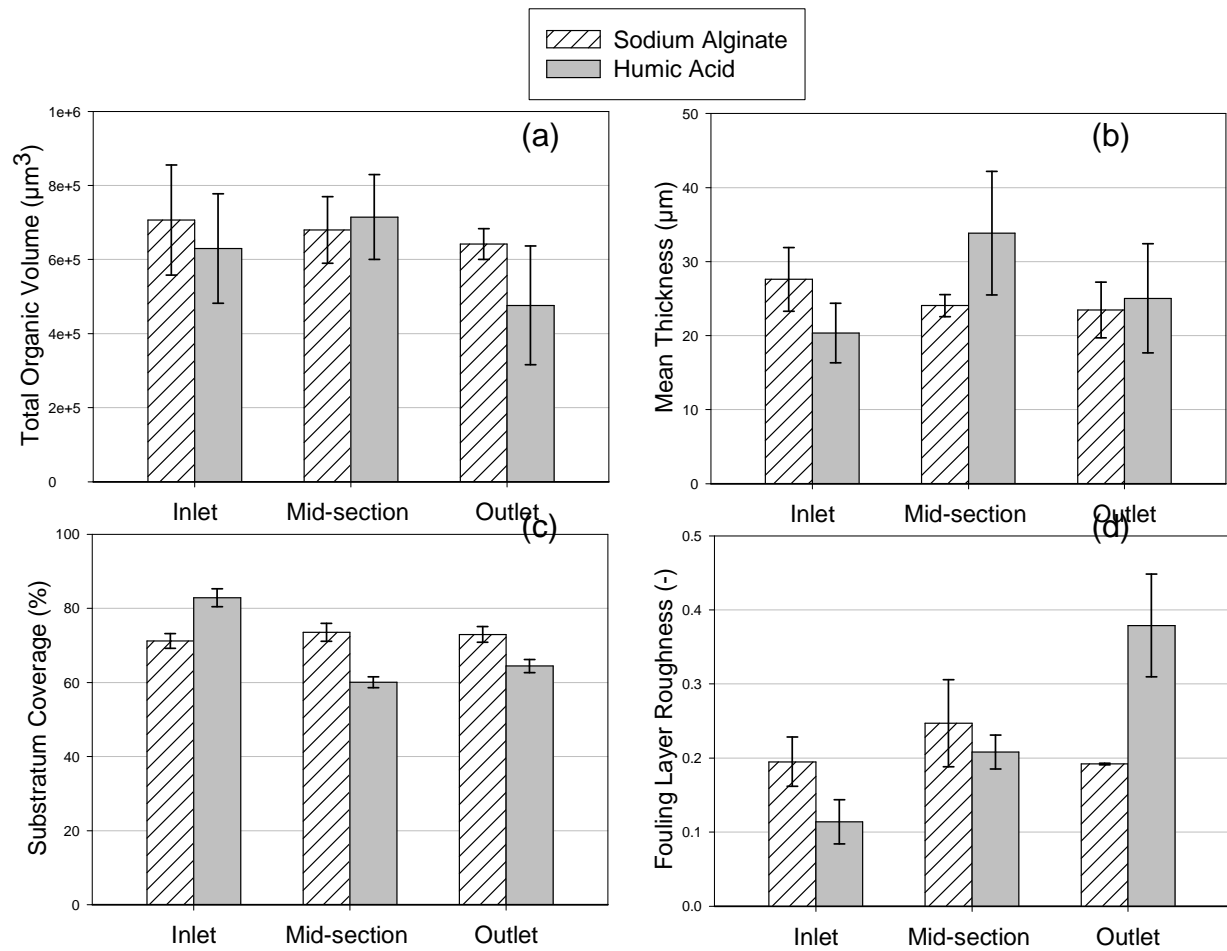


Figure 2: Confocal Microscopy results of NF90 membrane samples fouled with humic acid and alginic acid in cross-flow. Layer properties shown are: (a) total organic volume, (b) layer thickness, (c) surface coverage by the layer, (d) layer roughness. Fouling conditions: 42 LMH permeate flux, 0.39 m/s cross-flow rate. Feed solution: 1 mgC/L humic acid or 2 mgC/L alginic acid, 20 mM NaCl, 1 mM NaHCO₃ and 0.5mM CaCl₂, 20 ± 1 °C, pH 8.5.

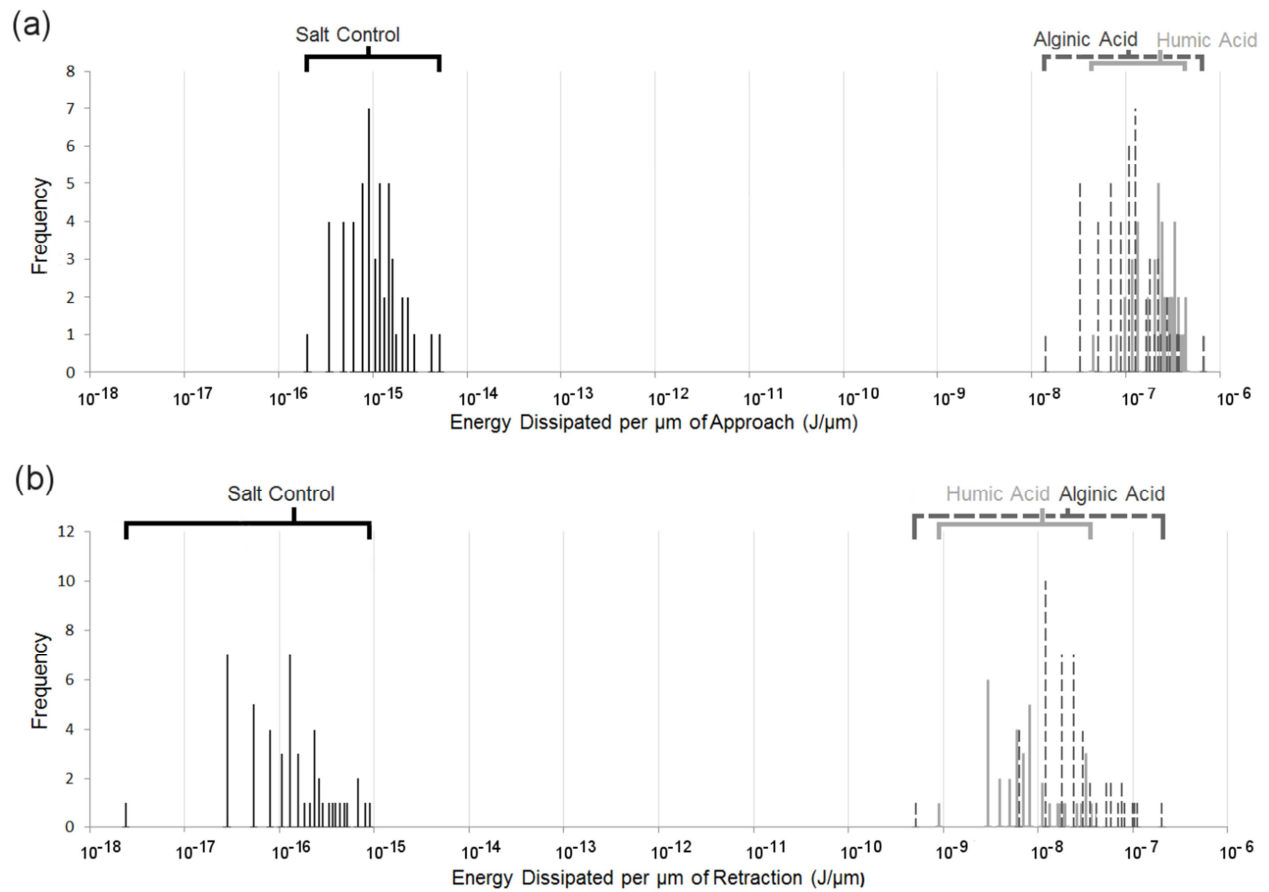


Figure 3: Population density diagrams of the energy dissipated during approach (a) and retraction (b) of a triangular silicon nitride Atomic Force Microscopy probe through the top 0.5 - 1 μm of fouling layers of humic acid and alginic acid on NF90 membranes, or within 0.5 μm of an unfouled salt control sample. 50 independent measurements were taken from 8 membrane samples for each foulant and corrected to 1 μm for comparative purposes. Energy dissipated is presented on a \log_{10} scale.

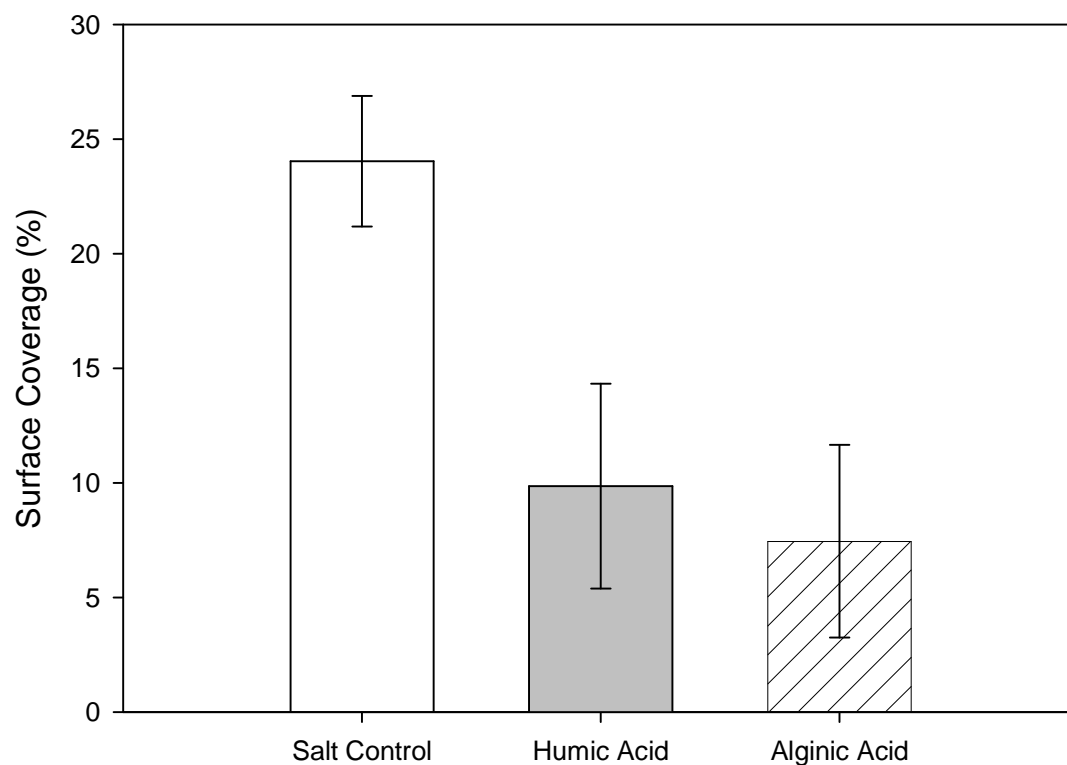


Figure 4: Surface coverage of *Pseudomonas fluorescens* cells on NF90 membrane samples fouled with humic acid, alginate acid and a salt control under cross-flow conditions after 30 minutes of initial adhesion (42 LMH permeate flux, 0.39 m/s cross-flow rate). Feed solution: 1mgC/L humic acid or 2mgC/L alginate acid, 20 mM NaCl, 1 mM NaHCO₃ and 0.5 mM CaCl₂, 20 ± 1 °C, pH 8.5. The results shown are the average of at least three samples from all regions of the membrane (inlet, mid-section and outlet) for each feed with the standard deviations shown.

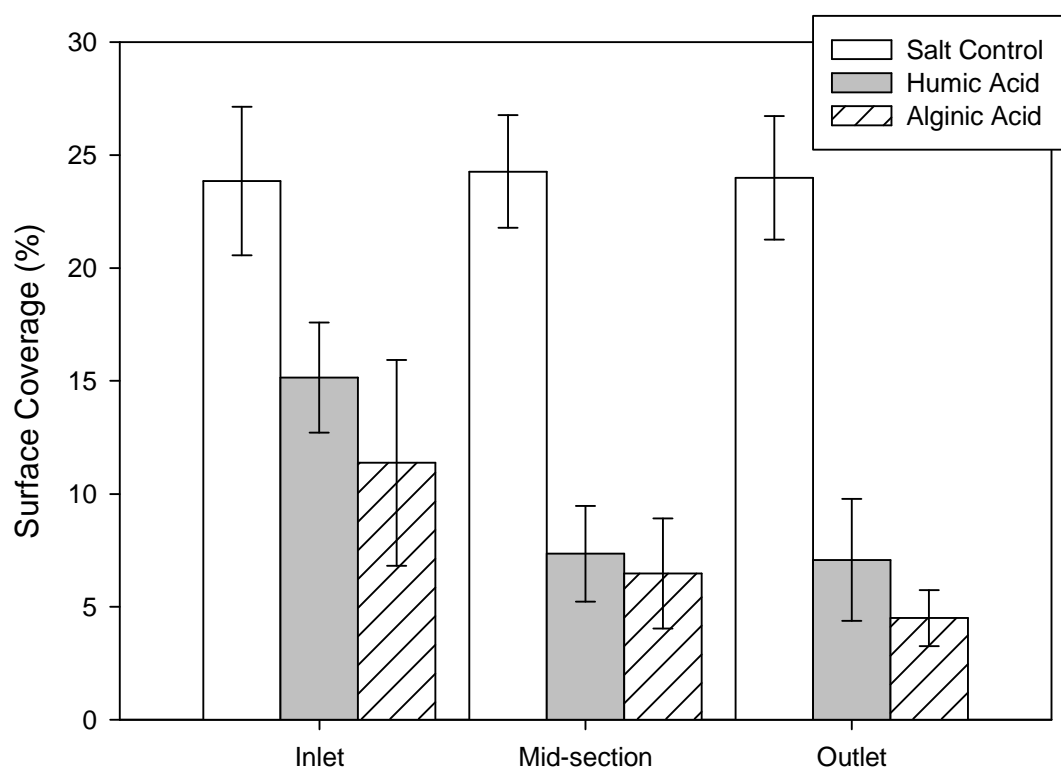


Figure 5: Surface coverage of *Pseudomonas fluorescens* cells on NF90 membrane samples fouled with humic acid, alginic acid and a salt control under cross-flow conditions (42 LMH permeate flux, 0.39 m/s cross-flow rate) after 30 minutes of initial adhesion. Feeds solution: 1mgC/L humic acid or 2mgC/L alginic acid, 20 mM NaCl, 1 mM NaHCO₃ and 0.5 mM CaCl₂, 20 ± 1 °C, pH 8.5. The results shown are the average of at least three samples from each region of the membrane (inlet, mid-section and outlet) for each feed with the standard deviations shown.